Lean-water Hydrogel with Multipolar Sites for Flexible and High-performance Aqueous Aluminum Ion Batteries

Ziyue Wen[a,b,c], Man-Fai Ng[d], Beier Jia[c], Jinxuan Song[c], Tianyang Yu[b], Jinfeng Dong[c], Anchun Tang[c], Yuansheng Shi[c], Renjie Chen[b,*] and Qingyu Yan[c,*]

a. School of New Energy, North China Electric Power University, Beijing102206, China.

b. School of Material Science & Engineering, Beijing Key Laboratory of Environmental Science and Engineering, Beijing Institute of Technology, Beijing100081, China.

c. School of Materials Science and Engineering, Nanyang Technological University, Singapore, Singapore.

d. Institute of High Performance Computing (IHPC), Agency for Science, Technology and Research (A*STAR), 1 Fusionopolis Way, #16-16 Connexis, Singapore 138632, Republic of Singapore.

*Corresponding author：

Email address: alexyan@ntu.edu.sg; chenrj@bit.edu.cn

Abstract

Rechargeable aqueous aluminum ion batteries (AAIBs) offer a promising avenue for achieving safe, high-energy and low-cost large-scale energy storage applications. However, the practical development of AAIBs is hindered by competitive reduction reactions in the aqueous solution, which lead to insufficient aluminum (Al) deposition and a severe hydrogen evolution reaction (HRE). In this work, an inorganic/organic hybrid hydrogel with a stable silicon-based network and multiple polar sites was successfully fabricated via an in-situ sol-gel polymerization method. The preferential formation of hydrogen bonds between the polar functional groups (-C=O and -NH) and water molecules effectively reduces the thermodynamic reactivity of water. Furthermore, X-ray photoelectron spectroscopy (XPS) and time of flight secondary ion

mass spectrometry (TOF-SIMS) analyses confirm the formation of a stable, inorganic-rich solid electrolyte interface (SEI) layer, which kinetically suppresses undesirable side reactions. This hydrogel electrolyte exhibits a high ionic conductivity of 2.9×10^{-3} S cm^{-1} at 25 ℃, even under lean-water conditions. As a result, Al|hydrogel|KNHCF full cells demonstrate excellent cycling performance, delivering a high initial discharge capacity of 74.9 mAh g^{-1} at 100 mA g^{-1} and achieving an outstanding capacity retention of 90.0 % after 200 cycles. Additionally, pouch cells exhibit stable open-circuit voltage under various mechanical abuse conditions. This work provides a promising approach for designing hydrogel electrolytes to enable high-performance and flexible AAIBs.

Introduction

With the growing demand for sustainable energy, lithium-ion batteries have emerged as the predominant power supplies for electric vehicles and portable electronic devices.[1-4] However, due to limited lithium resources and safety issues, it is imperative to explore next-generation electrochemical storage systems.[5-6] Aqueous aluminum ion batteries (AAIBs) exhibit promising prospects for large-scale energy storage due to high specific capacity (8035 mAh cm^{-3}, 2976 mAh g^{-1}), high abundance, and inherent safety characteristics of aluminum (Al) metal anode.[7-10] Currently in the early stages of development, AAIBs confront several challenges that require attention, particularly regarding the electrolyte/Al anode interface.[7, 11] Specifically, the reversible electrochemical deposition of Al is hindered in traditional aqueous electrolytes due to the competitive reduction between Al^{3+}/Al (-1.66 V vs standard hydrogen electrode) and H^{+}/H_2, leading to a parasitic hydrogen evolution rection (HER).[12-13] Thus, it is urgent to design electrolytes with a wide electrochemical stability window (ESW) in order to suppress water decomposition and Al anode corrosion.

To date, various strategies have been employed to inhibit HER in aqueous electrolytes, such as "water-in-salt" concept[14-15] and incorporation of functional additives or organic solvents.[16-19] These approaches aim to reduce water reactivity by modulating the solvation structure, thereby alleviating interfacial side reactions.[20-22] Despite advancements in regulating aqueous electrolytes, several challenges remain for

further development of rechargeable AAIBs: 1) suppression of side reactions at the anode surface; 2) inherent evaporation and leakage of liquid electrolytes; and 3) compromised mechanical stability of electrode/electrolyte interface under external force strain.[23-24] In contrast, gel polymer electrolytes are widely recognized for their superior leak resistance and enhanced flexibility.[25-28] However, their complex preparation processes and associated environmental concerns pose limitations on their large-scale development and commercialization. Hydrogel electrolytes (HEs), particularly those based on inorganic Si-O-Si networks, show considerable potential due to their low cost, non-toxic nature, and easy-scale-up preparation.[29-33] Moreover, the abundant hydrophilic groups within hydrogel networks can effectively alter the hydrogen bond interactions in water, thereby inhibiting side reactions.[34-36] Nevertheless, their application in AAIBs has been rarely explored to date. At this stage of AAIBs development, there is an urgent need to design high-performance hydrogels that exhibit exceptional physicochemical and electrochemical properties, which are considered pivotal for the realization of wearable battery systems.

In this study, we developed a novel hydrogel electrolyte for AAIBs using aluminum trifluoromethanesulfonate ($Al(OTF)_3$) as the Al salt, 1-[3-(trimethoxysilyl)propyl]urea (TU) and tetraethyl orthosilicate (TEOS) as crosslinkers. During the preparation process, TU and TEOS undergo copolymerization to form an inorganic/organic hybrid three-dimensional (3D) structure. This copolymerization occurs via hydrolysis and condensation reactions in an acidic $Al(OTF)_3/H_2O$ solution, without requiring additional catalysts. Numerous polar groups promote the aggregation of H_2O molecules around the Si-O-Si chains, while strongly electronegative carboxyl oxygen atoms establish ion transport channels, facilitating rapid ion migration under lean-water conditions (Figure 1a). Density functional theory (DFT) calculations and Fourier transform infrared (FTIR) analyses reveal that the abundant polar functional groups (-C=O and -NH) in this hydrogel tend to form hydrogen bonds with H_2O molecules. This disrupts the native hydrogen bond network of water, effectively reducing water activity and enhancing electrolyte stability. As a result, a wider ESW of 2.65 V (vs Al^{3+}/Al) is achieved, outperforming the liquid electrolyte (LE, 2M $Al(OTF)_3/H_2O$). Notably, in-

situ differential electrochemical mass spectrometry (DEMS) and optical microscopy tests clearly demonstrate the effective suppression of HER. Besides, the hydrogel achieves an ionic conductivity of 2.9×10^{-3} S cm^{-1} at 25 ℃, even with a water content as low as 23 wt%, owing to the presence of fast ion transport pathways. Therefore, both Al|HE|Al and Al|HE|KNHCF cells exhibit outstanding cycling performance. This hydrogel, with its unique molecular structure, presents a promising pathway for the development of eco-friendly, low-cost and high-performance AAIBs.

Results and discussion

The interaction between hydrogel chains and water was investigated using DFT analysis. The electrostatic potential (ESP) distribution was initially analyzed to visualize the electronegative and electropositive regions within the TU molecule (Figure 1b). The negative region near the carboxyl oxygen atom and the positive region associated with the amino hydrogen atom suggest that the former can serve as a hydrogen bond acceptor, while the latter can function as a hydrogen bond donor. To quantify these interactions, the binding energies of H_2O-H_2O, H_2O-TU(O), and H_2O-TU(NH) were calculated, as shown in Figure 1c. Specifically, the binding energy of H_2O-TU(O) (0.23 eV) is notably higher than that of the H_2O-H_2O dimer (0.16 eV), indicating a stronger electrostatic interaction between H_2O and TU(O). Additionally, the binding energy of H_2O-TU(NH) (0.15 eV) is comparable to that of water dimers, suggesting a competitive interaction for hydrogen bonding between water and NH. This competition can also disrupt the hydrogen bond network among water molecules. These findings demonstrate the anchoring effect of polar functional groups in the Si-O-Si chains with water molecules, reducing the water activity, mitigating the HER, and contributing to the broadening of the ESW.

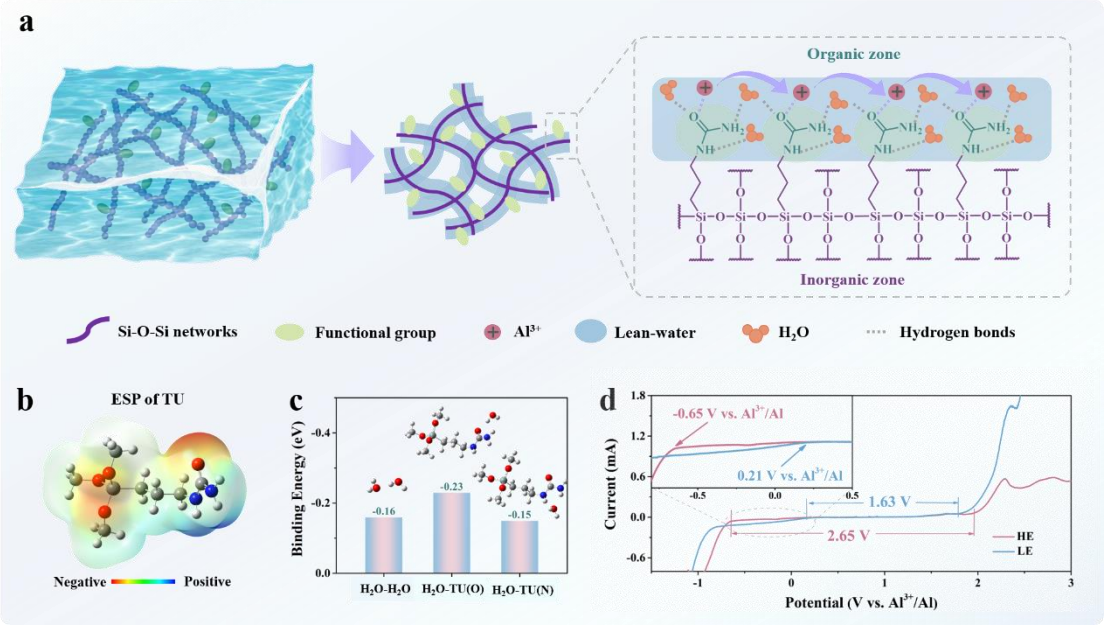

Figure 1 a) Schematic of the HE and molecular structure. b) ESP of TU. c) Calculated binding energies of H_2O-H_2O, H_2O-TU(O) and H_2O-TU(NH). d) LSV profiles of HE and LE at a scan rate of 0.5 mV s^{-1}. Inset: magnification diagram of hydrogen evolution potential.

Linear sweep voltammetry (LSV) measurements were performed to experimentally validate the theoretical findings. Stainless steel (SS)|electrolyte|Al cells were assembled for this purpose, where SS served as the work electrode and Al foil functioned as both the counter and reference electrodes. As shown in Figure 1d, the hydrogel exhibits a significantly broader ESW of 2.65 V vs. Al^{3+}/Al, compared to that of aqueous liquid electrolyte (1.63 V vs. Al^{3+}/Al). Notably, its hydrogen evolution potential is approximately -0.65 V vs. Al^{3+}/Al, which is sufficiently low to enable reversible Al deposition. This result confirms that the polar group-based hydrogel effectively mitigates HER by forming hydrogen bonds with water, thereby reducing water reactivity and stabilizing the interface.

The optical photographs of the electrolyte before and after copolymerization are presented in Figure 2a. Following the incorporation of crosslinkers and the polymerization process, the hydrogel exhibits macroscopic morphological stability, which can be attributed to its unique 3D network structure. Additionally, the hydrogel exhibits good self-healing properties and mechanical flexibility, as shown in Figure 2b

and S1, highlighting its potential for enhancing battery safety and enabling wearable applications. The microstructure of the hydrogel skeleton was then investigated using scanning electron microscopy (SEM). It is clear that the Si-O-Si matrix forms a 3D network structure composed of numerous interconnected nanoparticles (Figure 2c). This porous morphology, combined with hydrophilic functional groups, facilitates the formation of fast Al^{3+} ion transport channels, enabling efficient ion migration within the electrolyte.

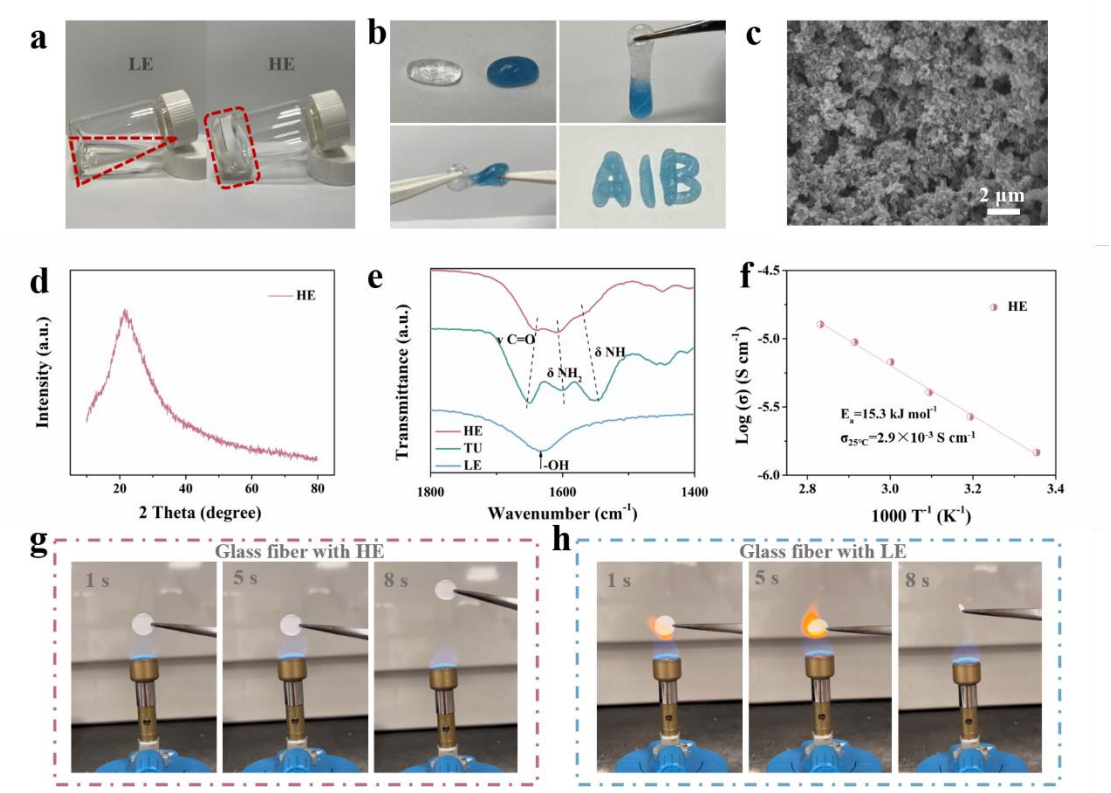

Figure 2 Optical photographs of a) LE, HE and b) self-healing properties and flexibility of hydrogel (hydrogel was mixed with blue ink to produce a blue hydrogel). c) The SEM image of the Si-O-Si networks. d) XRD spectrum of HE. e) FTIR spectra of LE, HE and TU. f) Ionic conductivity of HE from 25 to 80 ℃ obtained from electrochemical impedance spectroscopy. Digital images of combustion tests for glass fibers saturated with g) HE and h) LE.

The crystallinity of hydrogel synthesized via sol-gel polymerization was further analyzed using XRD. As shown in Figure 2d, the broad peak observed around 22° corresponds to the amorphous SiO_2. It is well established that amorphous SiO_2

possesses a large surface area, high pore volume, and good flexibility, thereby providing numerous active sites.[37-39] Hydrogel electrolytes can generally be classified into two types based on their cross-linking modes: chemical and physical, which are closely associated with their mechanical properties, thermal stability, reliability, and durability. In this work, the hydrogel is double-crosslinked through both physical (hydrogen bonds) and chemical (covalent bonds) interactions to form an amorphous structure. According to previous literature, double crosslinked hydrogels exhibit superior mechanical strength, flexibility, and stability compared to their single-crosslinked counterparts, making them highly advantageous for demanding electrochemical applications.[29, 40]

To further elucidate the hydrogen bond interactions between functional groups in hydrogel skeleton and H_2O molecules, FTIR tests were employed. In Figure 2e and S2, the peaks at approximately 1650 cm^{-1}, 1600 cm^{-1} and 1500 cm^{-1} correspond to the -C=O, -NH_2 and -NH- groups in TU, respectively. In the FTIR spectra of hydrogel, a red shift is observed in the stretching vibration of -C=O, while a blue shift appears in the bending vibration of -NH_2 and -NH-. These shifts are attributed to hydrogen bond interactions between the functional groups and H_2O, which is in consistent with our DFT calculations. Ionic conductivity is a crucial parameter for evaluating the application potential of electrolytes. Electrochemical impedance spectroscopy (EIS) tests were conducted in SS|hydrogel|SS cells. Interestingly, a high ionic conductivity of 2.9×10^{-3} S cm^{-1} at 25 ℃ can be obtained even under the lean-water conditions with a water content of 23 wt% (Figure S3). As depicted in Figure 1a, the abundant polar groups promote the aggregation of H_2O molecules around the Si-O-Si chains, facilitating rapid ion migration along the carboxyl oxygen atoms even at reduced water content. Besides, the activation energy (E_a), calculated from the Arrhenius plots via linear fitting, is determined to be 15.3 kJ mol^{-1}, indicating a low migration barrier for Al^{3+} ions within the hydrogel (Figure 2f and Table S3). This result highlights the hydrogel's ability to maintain efficient ion transport, which is critical for high-performance AAIBs.

Combustion tests were conducted to evaluate the flammability and safety of the hydrogel. In this test, glass fibers were immersed in the hydrogel precursor solution and

subsequently underwent a polymerization process. Ignition tests were then performed to assess the flame resistance. As depicted in Figure 2g, no burning occurred even when the ignition time is extended to 8 s. This excellent flame retardancy can be attributed to the strong Si-O bonds within the hydrogel matrix and the release of inert N_2 generated from the thermal decomposition of amino groups. In contrast, the glass fiber soaked with LE exhibited combustibility (Figure 2h). This result indicates the insufficient flame retardancy of the LE, which is unable to inhibit burning of glass fiber under the same conditions. These findings demonstrate the hydrogel's significant safety advantages, making it a more suitable choice for next-generation energy storage systems, particularly in applications where thermal stability and safety are critical.

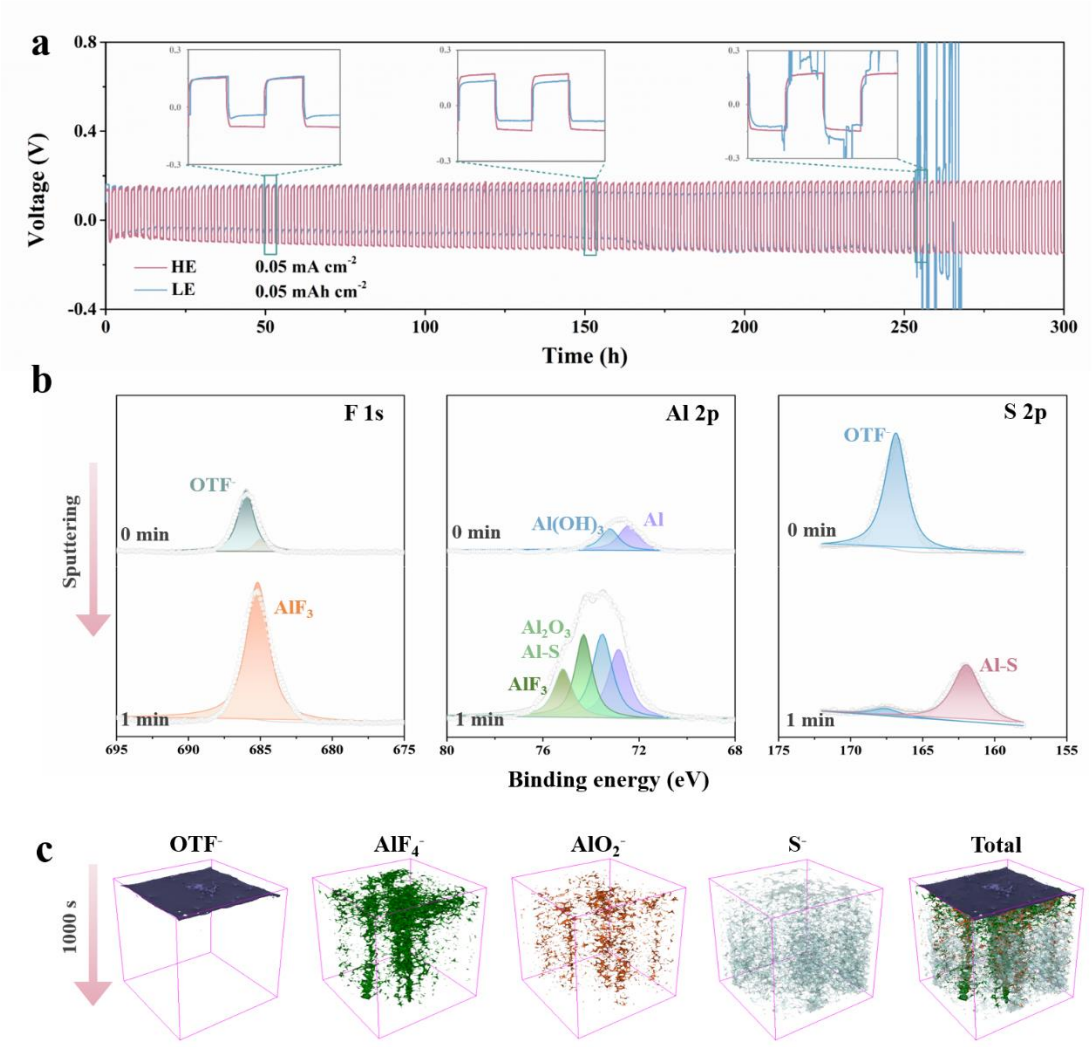

Figure 3 a) Galvanostatic charge/discharge profiles of symmetrical Al||Al batteries at a current density of 0.05 mA cm^{-2} and areal capacity of 0.05 mAh cm^{-2}. Inset:

magnification cycling performance of 50-54 h, 150-154 h and 253-257 h. b) In-depth XPS spectra of F 1s, Al 2p and S 2p from cycled Al metal. c) ToF-SIMS analysis of cycled Al metal.

The plating and stripping behavior of the Al was investigated through galvanostatic charge/discharge tests on symmetrical cells. Figure 3a presents the cycling performance of the Al|HE|Al cell at a current density of 0.05 mA cm^{-2}, with the Al|LE|Al cell serving as the control sample. In the Al|LE|Al cell, a fluctuating overpotential is observed, and the cell suddenly fails after 250 h of cycling. This behavior indicates uneven and irreversible Al plating in the aqueous liquid electrolyte due to side reactions and poor electrode compatibility. In contrast, the symmetrical cell based on HE exhibits stable voltage polarization profiles (~ 0.15 V) over 300 h, demonstrating the reversible and uniform deposition/stripping of Al, with reduced side reactions. To further confirm the interfacial behavior, the microstructure of Al electrode cycled in the HE was then examined using SEM. The SEM image displays a smooth and dense Al surface without dendrite formation, proving clear evidence of the hydrogel's ability to enable uniform and reversible plating/stripping (Figure S4). In short, these results highlight that the hydrogel employed in this work effectively mitigates side reactions and enhances the reversibility of Al deposition/stripping in AAIBs.

To further elucidate the protective mechanism at the Al/HE interface, in-depth XPS and TOF-SIMS techniques were performed to study the composition and structure of SEI. Following 50 h of cycling, the Al electrode was disassembled from the Al|HE|Al cell. XPS tests were initially conducted. As shown in Figure 3b, XPS spectra reveal that the outside layer of the Al electrode primarily consists of residual $Al(OTF)_3$ salt. Following a 1 min etching process, the SEI layer was found to be dominated by inorganic components, including Al-F, Al-S, and Al-O species. Further insights into the interface behavior were obtained through TOF-SIMS analysis, which provided 3D spatial distribution of the SEI structure. As shown in Figure 3c, residual OTF^- is observed on the surface. The AlF_4^-, AlO_2^- and S^- secondary ions are detected within the SEI layer, which is consistent with the XPS results (Figure S5 and S6). These components are primarily attributed to the preferential reductive decomposition of

OTF^- anions. It is widely acknowledged that the parasitic HER in aqueous electrolyte can be kinetically suppressed though the formation of an SEI enriched with inorganic components.[15] Such an SEI serves as a protective barrier, promoting Al nucleation and uniform deposition while avoiding direct contact between water and Al metal, thereby mitigating side reactions and facilitating long-term cycling performance.[41]

To visually observe the HER in both hydrogel and liquid electrolyte systems, we conducted in-situ DEMS measurements on Al||potassium nickel hexacyanoferrate (KNHCF) full cells to record the H_2 evolution during the first three cycles. As shown in Figure 4a, a pronounced H_2 evolution signal was detected during each charging process in the liquid electrolyte, indicating severe water decomposition occurring prior to Al deposition. In contrast, HER was effectively suppressed in the hydrogel-based cell, with reduced H_2 generation observed during cycling (Figure 4b). These findings were further supported by in-situ optical microscopy tests, which provided a real-time observation of gas evolution at the interface. The optical images of gas evolution in the Al|LE|Al and Al|HE|Al batteries at a current density of 0.3 mA cm^{-2} are shown in Figure 4c and d, respectively. Continuous bubbles were observed in the liquid electrolyte from 1 to 10 minutes, confirming the severe HER during cell operation (Figure 4c). In contrast, minimal bubble generation was observed at the Al|HE interface under the same current density, which is consistent with the results obtained from in-situ DEMS analysis (Figure 4d). These results further demonstrate the ability of the hydrogel to effectively mitigate water decomposition at the Al/electrolyte interface. This stabilization is critical for enabling highly efficient and reversible Al deposition, thus contributing to the long-term cycling stability of AAIBs.

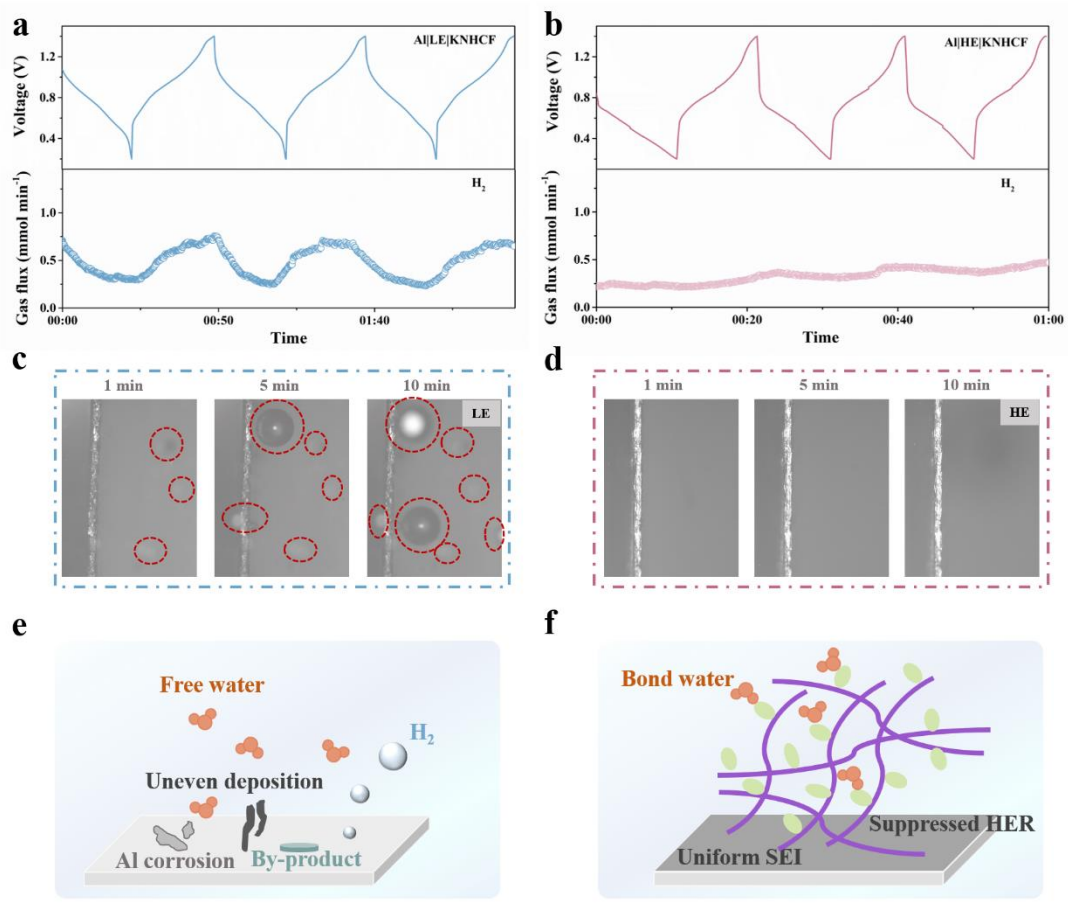

Figure 4 In-situ DEMS testing for a) Al|LE|KNHCF and b) Al|HE|KNHCF. Optical images of gas evolution in the c) Al|LE|Al cell and d) Al|HE|Al cell at 0.3 mA cm^{-2} by in-situ optical microscope. Schematic illustrations of Al interface in the e) LE and f) HE.

Based on these in-situ tests, we propose that the mitigated HER in the hydrogel system can be attributed to a combination of thermodynamic and kinetic protective mechanisms: 1) Thermodynamically, the formation of hydrogen bonds between the polar functional groups in the Si-O-Si chains and H_2O molecules effectively reduces water reactivity, thereby suppressing HER; 2) Kinetically, a stable and robust SEI, induced by the hydrogel, promotes uniform deposition of Al while avoiding direct contact between water and Al metal, thus mitigating side reactions. As illustrated in Figure 4e and f, the combined effects of increased bonded water and the formation of a stable SEI result in remarkable inhibition of HER. Benefitting from these two mechanisms, reversible electrochemical performance can be achieved.

The Al||KNHCF full batteries were fabricated to evaluate the long-term electrochemical performance. The Nyquist plots of the fresh full cell are shown in Figure S7. At a current density of 100 mA g^{-1}, the Al|HE|KNHCF cell exhibits outstanding cycling stability, delivering an initial discharge capacity of 74.9 mAh g^{-1} with a high average Coulombic efficiency of 99.6 % (Figure 5a). After 200 cycles, the capacity retention remains at 90.0 %. In sharp contrast, the LE-based full cell exhibits low specific discharge capacity and accelerated capacity degradation. In detail, only 27.8 % of its initial capacity is retained after 200 cycles, which caused by the continuous side reactions. Figure 5b compares the appearance of the coin cells after cycling. It can be clearly seen that the LE-based coin cell visibly ruptured due to pronounced H_2 evolution during cycling, while the Al|HE|KNHCF coin cell remained largely intact. This can be attributed to the unique hydrogel design, which suppresses HER and stabilizes the SEI layer. The corresponding charge/discharge profiles of 40^{th} cycle in Figure 5c show the small voltage polarization and a stable voltage plateau. A higher specific discharge capacity (~ 68 mAh g^{-1}) is achieved compared to most previously reported AAIBs utilizing Prussian blue analogue cathodes.

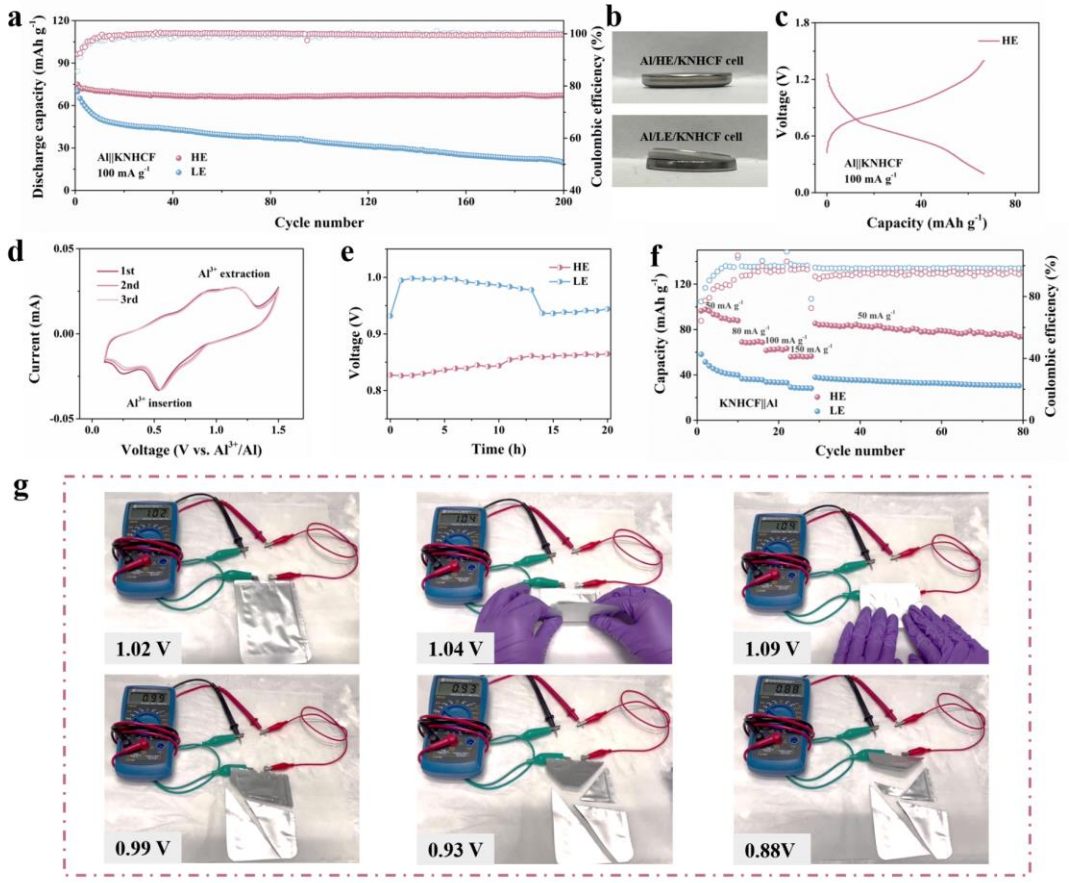

Figure 5 a) Cycling performance of Al||KNHCF full cells at a current density of 100 mA g^{-1} with HE and LE. b) Digital photos of coin cells after cycling. c) Corresponding charge/discharge capacity-voltage curves of the 40th cycle. d) Cyclic voltammetry curves of Al|HE|KNHCF full cell at a scan rate of 0.3 mV s^{-1}. e) OCV decay with time. f) Rate performance of Al||KNHCF full cells at current densities of 50, 80, 100 and 150 mA g^{-1}. g) OCV of the Al|HE|KNHCF punch cell under bending, folding and cutting.

Figure 5d presents the cyclic voltammetry (CV) curves of the Al|HE|KNHCF full cell at a scan rate of 0.3 mV s^{-1} within the voltage range of 0.1-1.5 V . It is noteworthy that the oxidation and reduction peaks correspond to the Al^{3+} extraction and insertion processes, respectively. Besides, there is no obvious alteration are observed in the CV curves during the first three cycles, which can be attributed to the low polarization and the presence of large ion channels in KNHCF cathode. To evaluate the internal stability of the cell, the self-discharge process was monitored over a resting period of 20 h. The open circuit voltage (OCV) of the Al|LE|KNHCF full cell exhibits a gradual decrease

within the first 12 h of standing, as depicted in Figure 5e. A sudden drop occurred at 13 h, indicating persistent internal self-discharge (associated with side reactions) and poor compatibility between the aqueous electrolyte and electrode materials. In contrast, the HE-based cell maintained a constant OCV throughout the resting period, signifying a stable hydrogel and interface. The rate performance of the Al|HE|KNHCF full cell was further assessed across a range of current densities from 50 to 150 mA g^{-1} (Figure 5f). The cell demonstrates average discharge capacities of 92.0, 68.8, 62.4 and 56.1 mAh g^{-1} at current densities of 50, 80, 100 and 150 mA g^{-1}, respectively, which significantly outperform those of LE-based full cell. Importantly, when the current density was returned to 50 mA g^{-1}, the capacity recovered to 85.3 mAh g^{-1}. The corresponding charge/discharge curves, as presented in Figure S8, exhibit good electrochemical performance with respect to specific capacity and voltage plateau.

Finally, pouch cells were constructed to evaluate the flexibility and safety of the Al|HE|KNHCF (Figure 5g) and Al|HE|Al_xMnO_2 (Figure S9) systems under various mechanical stresses. As displayed in Figure 5g, the Al|HE|KNHCF pouch cell exhibited an OCV of 1.02 V under normal conditions. Remarkably, its OCV remained stable even after subjecting the pouch cell to bending (90°) and folding (180°), highlighting its excellent mechanical flexibility. Moreover, when the pouch was cut into pieces, only a slight reduction in OCV was observed, and no signs of electrolyte leakage or short-circuiting were detected. Owing to its inherent stable physical and chemical properties, the aqueous silicon-based hydrogel maintained a normal OCV when exposed to air, thereby demonstrating its potential for achieving flexible and high safety AAIBs.

Conclusions

In conclusion, we developed a novel hydrogel with a rapid ion conduction pathway via in-situ sol-gel polymerization. DFT calculations, combined with FTIR spectroscopy, reveal that the polar groups in the hydrogel skeleton form hydrogen bonds with H_2O molecules, disrupting the native hydrogen bond network in water and inhibiting the HER. By exploiting this mechanism, LSV tests demonstrates a wide ESW of 2.65 V vs Al^{3+}/Al. In-situ DEMS and optical microscopy tests further provide direct evidence of

the effective suppression of hydrogen evolution. In addition, even under lean-water conditions, the hydrogel exhibits a high ionic conductivity of 2.9×10^{-3} S cm^{-1} due to the rapid ion migration pathway. Therefore, the Al||Al symmetrical cell achieves stable cycling with a low and consistent polarization potential of approximately 0.15 V at a current density of 0.05 mA cm^{-2} for over 300 h, indicating a reversible and uniform Al deposition/stripping process. The HE-based Al||KNHCF full cell also exhibits stable cycling performance with an impressive capacity retention of 90.0 % after 200 cycles. Finally, pouch cells were fabricated to assess their flexibility and safety under mechanical stresses. This work provides a path for the development of high-performance and flexible AAIBs for practical applications.

Acknowledgements

This work was supported by the ASTAR MTC programmatic project (M23L9b0052), Indonesia-NTU Singapore Institute of Research for Sustainability and Innovation (INSPIRASI) (6635/E3/KL.02.02/2023), Singapore NRF Singapore-China flagship program (023740-00001), the National Key Research and Development Program of China (2022YFB2502102) and Beijing Outstanding Young Scientists Program (BJJWZYJH01201910007023). We acknowledge the National Supercomputing Center (NSCC) Singapore and Agency for Science, Technology and Research (A*STAR) Computational Resource Centre (A*CRC) of Singapore for the use of its high-performance computing facilities.

Conflict of interest

The authors declare no conflict of interest.

Reference

1. Armand, M.; Tarascon, J. M., Building better batteries. *Nature* **2008,** *451* (7179), 652-657.
2. Trahey, L.; Brushett, F. R.; Balsara, N. P.; Ceder, G.; Cheng, L.; Chiang, Y.-M.; Hahn, N. T.; Ingram, B. J.; Minteer, S. D.; Moore, J. S., Energy storage emerging: A perspective from the Joint Center for Energy Storage Research. *Proceedings of the National Academy of Sciences* **2020,** *117* (23), 12550-12557.
3. Winter, M.; Barnett, B.; Xu, K., Before Li Ion Batteries. *Chemical Reviews* **2018,**

118 (23), 11433-11456.
4. Piątek, J.; Afyon, S.; Budnyak, T. M.; Budnyk, S.; Sipponen, M. H.; Slabon, A., Sustainable Li-ion batteries: chemistry and recycling. *Advanced Energy Materials* **2021,** *11* (43), 2003456.
5. Tian, Y.; Zeng, G.; Rutt, A.; Shi, T.; Kim, H.; Wang, J.; Koettgen, J.; Sun, Y.; Ouyang, B.; Chen, T.; Lun, Z.; Rong, Z.; Persson, K.; Ceder, G., Promises and Challenges of Next-Generation "Beyond Li-ion" Batteries for Electric Vehicles and Grid Decarbonization. *Chemical Reviews* **2021,** *121* (3), 1623-1669.
6. Deng, D., Li-ion batteries: basics, progress, and challenges. *Energy Science & Engineering* **2015,** *3* (5), 385-418.
7. Jiang, M.; Fu, C.; Meng, P.; Ren, J.; Wang, J.; Bu, J.; Dong, A.; Zhang, J.; Xiao, W.; Sun, B., Challenges and Strategies of Low-Cost Aluminum Anodes for High-Performance Al-Based Batteries. *Advanced materials* **2022,** *34* (2), e2102026.
8. Jia, B.-E.; Thang, A. Q.; Yan, C.; Liu, C.; Lv, C.; Zhu, Q.; Xu, J.; Chen, J.; Pan, H.; Yan, Q., Rechargeable Aqueous Aluminum-Ion Battery: Progress and Outlook. *Small* **2022,** *18* (43), 2107773.
9. Du, K.; Sun, C.-H.; Su, J.-W.; Zhao, Y.-Q.; Hou, J.-W.; Hu, Y.-X., Paving pathway for reliable cathodes development in aqueous aluminum-ion batteries: a mini review. *Rare Metals* **2024,** *43* (12), 6164-6182.
10. Xing, Z.; Wang, S.; Yu, A.; Chen, Z., Aqueous intercalation-type electrode materials for grid-level energy storage: Beyond the limits of lithium and sodium. *Nano Energy* **2018,** *50*, 229-244.
11. Yan, C.; Lv, C.; Jia, B. E.; Zhong, L.; Cao, X.; Guo, X.; Liu, H.; Xu, W.; Liu, D.; Yang, L.; Liu, J.; Hng, H. H.; Chen, W.; Song, L.; Li, S.; Liu, Z.; Yan, Q.; Yu, G., Reversible Al Metal Anodes Enabled by Amorphization for Aqueous Aluminum Batteries. *Journal of the American Chemical Society* **2022,** *144* (25), 11444-11455.
12. Hu, E.; Jia, B.-E.; Zhu, Q.; Xu, J.; Loh, X. J.; Chen, J.; Pan, H.; Yan, Q., Engineering High Voltage Aqueous Aluminum-Ion Batteries. *Small n/a* (n/a), 2309252.
13. Meng, P.; Yang, Z.; Zhang, J.; Jiang, M.; Wang, Y.; Zhang, X.; Luo, J.; Fu, C., Electrolyte design for rechargeable aluminum-ion batteries: Recent advances and challenges. *Energy Storage Materials* **2023,** *63*, 102953.
14. Xu, J.; Ji, X.; Zhang, J.; Yang, C.; Wang, P.; Liu, S.; Ludwig, K.; Chen, F.; Kofinas, P.; Wang, C., Aqueous electrolyte design for super-stable 2.5 V LiMn2O4 || Li4Ti5O12 pouch cells. *Nature Energy* **2022,** *7* (2), 186-193.
15. Suo, L.; Borodin, O.; Gao, T.; Olguin, M.; Ho, J.; Fan, X.; Luo, C.; Wang, C.; Xu, K., "Water-in-salt" electrolyte enables high-voltage aqueous lithium-ion chemistries. *Science* **2015,** *350* (6263), 938-943.
16. Zhao, Z.; Zhang, Z.; Wang, W.; Xu, T.; Yu, X., Strengthen Water O−H Bond in Electrolytes for Enhanced Reversibility and Safety in Aqueous Aluminum Ion Batteries. *Angewandte Chemie International Edition* **2024**.
17. Wang, T.; Tian, Z.; You, Z.; Li, Z.; Cheng, H.; Li, W.; Yang, Y.; Zhou, Y.; Zhong, Q.; Lai, Y., Hydrogen-bond network manipulation of aqueous electrolytes with high-donor solvent additives for Al-air batteries. *Energy Storage Materials* **2022,** *45*, 24-32.
18. Xie, J.; Liang, Z.; Lu, Y. C., Molecular crowding electrolytes for high-voltage

aqueous batteries. *Nature materials* **2020,** *19* (9), 1006-1011.
19. You, C.; Wu, R.; Yuan, X.; Liu, L.; Ye, J.; Fu, L.; Han, P.; Wu, Y., An inexpensive electrolyte with double-site hydrogen bonding and a regulated Zn2+ solvation structure for aqueous Zn-ion batteries capable of high-rate and ultra-long low-temperature operation. *Energy & Environmental Science* **2023,** *16* (11), 5096-5107.
20. Li, X.; Wang, X.; Ma, L.; Huang, W., Solvation Structures in Aqueous Metal-Ion Batteries. *Advanced Energy Materials* **2022,** *12* (37), 2202068.
21. Xu, Y.; Ma, J.; Jiang, T.; Ding, H.; Wang, W.; Wang, M.; Zheng, X.; Sun, J.; Yuan, Y.; Chuai, M.; Chen, N.; Li, Z.; Hu, H.; Chen, W., Tuning electrolyte solvation structures to enable stable aqueous Al/MnO2 battery. *Energy Storage Materials* **2022,** *47*, 113-121.
22. Zhao, Z.; Zhang, Z.; Xu, T.; Wang, W.; Wang, B.; Yu, X., Solvation Structure Regulation for Highly Reversible Aqueous Al Metal Batteries. *Journal of the American Chemical Society* **2024,** *146* (3), 2257-2266.
23. Dong, T.; Ng, K. L.; Wang, Y.; Voznyy, O.; Azimi, G., Solid Electrolyte Interphase Engineering for Aqueous Aluminum Metal Batteries: A Critical Evaluation. *Advanced Energy Materials* **2021,** *11* (20).
24. Yu, H.; Lv, C.; Yan, C.; Yu, G., Interface Engineering for Aqueous Aluminum Metal Batteries: Current Progresses and Future Prospects. *Small Methods* **2024,** *8* (6), 2300758.
25. Shen, X.; Sun, T.; Wu, Z.; Tan, L., Ultrafast charging and ultralong cycle life in solid-state Al-ion batteries. *Journal of Materials Chemistry A* **2022,** *10* (15), 8178-8185.
26. Yu, Z.; Jiao, S.; Li, S.; Chen, X.; Song, W. L.; Teng, T.; Tu, J.; Chen, H. S.; Zhang, G.; Fang, D. N., Flexible Stable Solid-State Al-Ion Batteries. *Advanced Functional Materials* **2018,** *29* (1).
27. Yu, Z.; Jiao, S.; Tu, J.; Song, W.-L.; Lei, H.; Jiao, H.; Chen, H.; Fang, D., Gel electrolytes with a wide potential window for high-rate Al-ion batteries. *Journal of Materials Chemistry A* **2019,** *7* (35), 20348-20356.
28. Yu, Z.; Wang, W.; Zhu, Y.; Song, W. L.; Huang, Z.; Wang, Z.; Jiao, S., Construction of double reaction zones for long-life quasi-solid aluminum-ion batteries by realizing maximum electron transfer. *Nature communications* **2023,** *14* (1), 5596.
29. Peng, H.; Wang, D.; Zhang, F.; Yang, L.; Jiang, X.; Zhang, K.; Qian, Z.; Yang, J., Improvements and Challenges of Hydrogel Polymer Electrolytes for Advanced Zinc Anodes in Aqueous Zinc-Ion Batteries. *ACS Nano* **2024,** *18* (33), 21779-21803.
30. Fan, X.; Zhang, R.; Sui, S.; Liu, X.; Liu, J.; Shi, C.; Zhao, N.; Zhong, C.; Hu, W., Starch-Based Superabsorbent Hydrogel with High Electrolyte Retention Capability and Synergistic Interface Engineering for Long-Lifespan Flexible Zinc-Air Batteries. *Angew Chem Int Ed Engl* **2023,** *62* (22), e202302640.
31. Gu, C.; Xie, X.-Q.; Liang, Y.; Li, J.; Wang, H.; Wang, K.; Liu, J.; Wang, M.; Zhang, Y.; Li, M.; Kong, H.; Liu, C.-S., Small molecule-based supramolecular-polymer double-network hydrogel electrolytes for ultra-stretchable and waterproof Zn–air batteries working from −50 to 100 °C. *Energy & Environmental Science* **2021,** *14* (8), 4451-4462.
32. Leng, K.; Li, G.; Guo, J.; Zhang, X.; Wang, A.; Liu, X.; Luo, J., A Safe

Polyzwitterionic Hydrogel Electrolyte for Long-Life Quasi-Solid State Zinc Metal Batteries. *Advanced Functional Materials* **2020,** *30* (23).
33. Liu, T.; Du, X.; Wu, H.; Ren, Y.; Wang, J.; Wang, H.; Chen, Z.; Zhao, J.; Cui, G., A Bio-Inspired Methylation Approach to Salt-Concentrated Hydrogel Electrolytes for Long-Life Rechargeable Batteries. *Angew Chem Int Ed Engl* **2023**, e202311589.
34. Wang, Y.; Li, Q.; Hong, H.; Yang, S.; Zhang, R.; Wang, X.; Jin, X.; Xiong, B.; Bai, S.; Zhi, C., Lean-water hydrogel electrolyte for zinc ion batteries. *Nature communications* **2023,** *14* (1), 3890.
35. Mo, F.; Chen, Z.; Liang, G.; Wang, D.; Zhao, Y.; Li, H.; Dong, B.; Zhi, C., Zwitterionic Sulfobetaine Hydrogel Electrolyte Building Separated Positive/Negative Ion Migration Channels for Aqueous Zn-MnO2 Batteries with Superior Rate Capabilities. *Advanced Energy Materials* **2020,** *10* (16).
36. Ma, R.; Xu, Z.; Wang, X., Polymer Hydrogel Electrolytes for Flexible and Multifunctional Zinc-Ion Batteries and Capacitors. *Energy & Environmental Materials* **2023,** *6* (5).
37. Tielens, F.; Gervais, C.; Lambert, J. F.; Mauri, F.; Costa, D., Ab Initio Study of the Hydroxylated Surface of Amorphous Silica: A Representative Model. *Chemistry of Materials* **2008,** *20* (10), 3336-3344.
38. Kresge, C. T.; Leonowicz, M. E.; Roth, W. J.; Vartuli, J. C.; Beck, J. S., Ordered mesoporous molecular sieves synthesized by a liquid-crystal template mechanism. *Nature* **1992,** *359* (6397), 710-712.
39. Giraldo, L. F.; López, B. L.; Pérez, L.; Urrego, S.; Sierra, L.; Mesa, M., Mesoporous Silica Applications. *Macromolecular Symposia* **2007,** *258* (1), 129-141.
40. Wang, X.; Wang, B.; Cheng, J., Multi-Healable, Mechanically Durable Double Cross-Linked Polyacrylamide Electrolyte Incorporating Hydrophobic Interactions for Dendrite-Free Flexible Zinc-Ion Batteries. *Advanced Functional Materials* **2023,** *33* (43), 2304470.
41. Chang, C.; Hu, S.; Li, T.; Zeng, F.; Wang, D.; Guo, S.; Xu, M.; Liang, G.; Tang, Y.; Li, H.; Han, C.; Cheng, H.-M., A robust gradient solid electrolyte interphase enables fast Zn dissolution and deposition dynamics. *Energy & Environmental Science* **2024,** *17* (2), 680-694.